International Journal of Engineering Science 49 (2011) 1311–1325

Contents lists available at ScienceDirect

International Journal of Engineering Science

journal homepage: www.elsevier.com/locate/ijengsci

Micromorphic approach to single crystal plasticity and damage

O. Aslan [a], N.M. Cordero [a], A. Gaubert [b], S. Forest [a,*]

[a] MINES ParisTech, Centre des matériaux, CNRS UMR 7633, BP 87, 91003 Evry Cedex, France
[b] Dept. of Metallic Materials and Structures, ONERA, 29 Avenue de la Division Leclerc, 92322 Châtillon Cedex, France

ARTICLE INFO

Article history:
Received 11 October 2010
Accepted 15 March 2011
Available online 20 April 2011

Keywords:
Crystal plasticity
Strain gradient plasticity
Cosserat medium
Micromorphic theory
Dislocation density tensor
Crack growth
Crack branching
Crack bifurcation

ABSTRACT

Eringen's micromorphic approach for materials with microstructure is applied to the plasticity and damage of single crystals. A plastic microdeformation variable and its rotational part are introduced in a standard crystal plasticity model in order to predict size effects in the overall stress response of crystalline solids. In the case of an ideal laminate microstructure including a purely elastic layer and a plastic layer undergoing single slip, the model, called *microcurl*, is shown to produce a kinematic hardening component that depends on the size of the layers. In a second part of the paper, a microdamage variable is introduced that accounts for cleavage or plasticity induced pseudo-cleavage phenomena in single crystals. The formulation accounts for straight crack paths but also allows for crack branching and bifurcation.

1. Introduction

The links between the micromorphic continuum and the plasticity of crystalline materials have been recognized very early by Eringen himself (Claus & Eringen, 1969; Eringen & Claus, 1970). Lattice directions in a single crystal can be regarded as directors that rotate and deform as they do in a micromorphic continuum. The fact that lattice directions can be rotated and stretched in a different way than material lines connecting individual atoms, especially in the presence of static or moving dislocations, illustrates the independence between directors and material lines in a micromorphic continuum, even though their deformations can be related at the constitutive level.

The identification of a micromorphic continuum from the discrete atomic single crystal model is possible based on suitable averaging relations proposed in Chen et al. (2003). These works contain virial formula for the higher order stress tensors arising in the micromorphic theory. This atomistic-based approach can be used to predict phonon dispersion relations (see also Claus & Eringen, 1971 for the study of dispersion of waves in a dislocated crystal).

Analytical solutions have been provided that give the generalized stress fields around individual screw or edge dislocations embedded in an elastic generalized continuum medium, like the micromorphic medium. The physical meaning of such a calculation is the account of non-local elasticity at the core of dislocations that may suppress or limit the singularity of the stress fields. For instance, non-singular force and couple stress were determined by Lazar and Maugin (2004) for a screw dislocation embedded in a gradient micropolar medium that combines the first strain gradient with independent rotational degrees of freedom. The unphysical singularities at the core of straight screw and edge dislocations are also removed when the second gradient of strain is introduced in the theory, while the first strain gradient is not sufficient (see Lazar, Maugin, & Aifantis, 2006).

* Corresponding author. Tel.: +33 1 60 76 30 51; fax: +33 1 60 76 31 50.
E-mail address: Samuel.Forest@ensmp.fr (S. Forest).

0020-7225/$ - see front matter © 2011 Elsevier Ltd. All rights reserved.
doi:10.1016/j.ijengsci.2011.03.008

The next step is to consider the collective behavior of dislocations in a single crystal by means of the continuum theory of dislocations. The material volume element is now assumed to contain a large enough number of dislocations for the continuum theory of dislocation to be applicable. Non-homogeneous plastic deformations induce material and lattice incompatibilities that are resolved by a suitable distribution of the dislocation density tensor field which is a second rank statistical mean for a population of arbitrary dislocations inside a material volume element (Kröner, 1969). Nye's fundamental relation linearly connects the dislocation density tensor to the lattice curvature field of the crystal. This fact has prompted many authors to treat a continuously dislocated crystal as a Cosserat continuum (Forest, Barbe, & Cailletaud, 2000; Günther, 1958; Kröner, 1963). The Cosserat approach records only the lattice curvature of the crystal but neglects the effect of the rotational part of the elastic strain tensor, which is a part of the total dislocation density tensor (Cordero et al., 2010). Full account of plastic incompatibilities is taken in strain gradient plasticity theories, starting from the original work by Aifantis (1984) up to recent progress by Gurtin (2002) and Acharya (2004). Formulation of crystal plasticity within the micromorphic framework is more recent and was suggested in Clayton, Bamman, and McDowell (2005) for a large spectrum of crystal defects, including point defects and disclinations. Limiting the discussion to dislocation density tensor effects, also called geometrically necessary dislocation (GND) effects, it is shown in Cordero et al. (2010), within a small deformation setting, how the micromorphic model can be used to predict grain and precipitate size effects in laminate crystalline materials. These models represent extensions of the conventional crystal plasticity theory (see for instance Teodosiu & Sidoroff, 1976), that accounts for single crystal hardening and lattice rotation but does not incorporate the effect of the dislocation density tensor.

The objective of the present work is, first, to formulate a finite deformation micromorphic extension of conventional crystal plasticity to account for GND effects in single crystals, and, second, to show that the micromorphic approach can also be used to introduce cleavage induced damage in a single crystal model. The first part, see Section 2, represents an extension to finite deformation of the model proposed by Cordero et al. (2010). It also provides new analytical predictions of size effects on the hardening of laminate microstructures. The theory is called the *microcurl* model because the evaluation of the curl of the microdeformation, instead of its full gradient, is sufficient to account for the effect of the dislocation density tensor. The second part, see Section 3, reports on a crystallographic model of damage in ductile single crystals, assuming that cracking occurs on specific crystallographic planes. The micromorphic approach is used here to obtain finite size damage zones and mesh-independent simulations of crack growth. In that way, the model is able to predict crack branching and bifurcation which are frequently observed in single crystals. It represents an extension to finite deformation and full coupling between plasticity and damage of the work initiated in Aslan and Forest (2009) and Aslan, Quilici, and Forest (2011).

The models proposed in this work for single crystals fall in the class of anisotropic elastoviscoplastic micromorphic media for which constitutive frameworks at finite deformations exist (Forest & Sievert, 2003; Lee & Chen, 2003; Regueiro, 2010; Sansour, Skatulla, & Zbib, 2010). The introduction of damage variables was performed in Grammenoudis, Tsakmakis, and Hofer (2009). In fact, the micromorphic approach can be applied not only to the total deformation by introducing the microdeformation field, but can also be restricted to plastic deformation, for specific application to size effects in plasticity, or to damage variables for application to regularized simulation of crack propagation, as proposed in Forest (2009) and Hirschberger and Steinmann (2009).

Vectors and second rank tensors are denoted by $\underset{\sim}{\boldsymbol{a}}, \boldsymbol{a}$, respectively. The theories are formulated within the general finite deformation framework essentially following Eringen's choice of strain measures (Eringen, 1999). The initial and current positions of the material point are denoted by $\underline{\boldsymbol{X}}$ and $\underline{\boldsymbol{x}}$, respectively. Throughout this work, the initial configuration of the body is V_0 whereas V denotes the current one. The associated smooth boundaries are ∂V_0 and ∂V with normal vector $\underline{\boldsymbol{N}}$ and $\underline{\boldsymbol{n}}$. The gradient operators with respect to initial and current coordinates are called $\boldsymbol{\nabla}_X$ and $\boldsymbol{\nabla}_x$, respectively. Similarly, the divergence and curl operators are Div, div and Curl, curl whether they are computed with respect to initial or current positions, respectively. Intrinsic notation is used in general but it is sometimes complemented or replaced by the index notation for clarity. A Cartesian coordinate system is used throughout with respect to the orthonormal basis $(\underline{\boldsymbol{e}}_1, \underline{\boldsymbol{e}}_2, \underline{\boldsymbol{e}}_3)$. The notations for double contraction and gradient operations are

$$\underset{\sim}{\boldsymbol{A}} : \underset{\sim}{\boldsymbol{B}} = A_{ij}B_{ij}, \quad \underline{\boldsymbol{u}} \otimes \boldsymbol{\nabla}_X = \frac{\partial u_i}{\partial X_j}\underline{\boldsymbol{e}}_i \otimes \underline{\boldsymbol{e}}_j \tag{1}$$

2. The *microcurl* model for crystal plasticity

2.1. Balance equations

The degrees of freedom of the proposed theory are the displacement vector $\underline{\boldsymbol{u}}$ and the microdeformation variable $\hat{\underset{\sim}{\boldsymbol{\chi}}}^p$, a generally non-symmetric second rank tensor. The field $\hat{\underset{\sim}{\boldsymbol{\chi}}}^p(\underline{\boldsymbol{X}})$ is generally not compatible, meaning that it does not derive from a vector field. The exponent ^{p} indicates, in advance, that this variable will eventually be constitutively related to plastic deformation occurring at the material point. In particular, the microdeformation $\hat{\underset{\sim}{\boldsymbol{\chi}}}^p$ is treated as an invariant quantity with respect to rigid body motion. The constitutive model will eventually ensure this invariance property. A first gradient theory is considered with respect to the degrees of freedom. However, the influence of the microdeformation gradient is limited to its curl part because of the aimed relation to the dislocation density tensor associated with the curl of plastic distortion. The following sets of degrees of freedom and of their gradients are therefore defined:

$$DOF = \left\{\underline{\boldsymbol{u}}, \hat{\underset{\sim}{\boldsymbol{\chi}}}^p\right\}, \quad GRAD = \left\{\underset{\sim}{\boldsymbol{F}} := \underset{\sim}{\boldsymbol{1}} + \underline{\boldsymbol{u}} \otimes \boldsymbol{\nabla}_X, \underset{\sim}{\boldsymbol{K}} := \operatorname{Curl} \hat{\underset{\sim}{\boldsymbol{\chi}}}^p\right\} \tag{2}$$

The following definition of the Curl operator is adopted, ϵ_{ijk} being the permutation tensor:

$$\operatorname{Curl}\underset{\sim}{\hat{\boldsymbol{\chi}}}^{p} := \frac{\partial \underset{\sim}{\hat{\boldsymbol{\chi}}}^{p}}{\partial X_k} \times \underline{\boldsymbol{e}}_k, \quad K_{ij} := \epsilon_{jkl}\frac{\partial \hat{\chi}^{p}_{ik}}{\partial X_l} \tag{3}$$

The method of virtual power is used to derive the balance and boundary conditions, following (Germain, 1973). For that purpose, we define the power density of internal forces as a linear form with respect to the velocity fields and their Eulerian gradients:

$$p^{(i)} = \underset{\sim}{\boldsymbol{\sigma}} : (\dot{\underline{\boldsymbol{u}}} \otimes \nabla_x) + \underset{\sim}{\boldsymbol{s}} : \dot{\underset{\sim}{\hat{\boldsymbol{\chi}}}}^{p} + \underset{\sim}{\boldsymbol{M}} : \operatorname{curl}\dot{\underset{\sim}{\hat{\boldsymbol{\chi}}}}^{p}, \quad \forall \underline{\boldsymbol{x}} \in V \tag{4}$$

where the conjugate quantities are the Cauchy stress tensor $\boldsymbol{\sigma}$, which is symmetric for objectivity reasons, the microstress tensor, $\underset{\sim}{\boldsymbol{s}}$, and the generalized couple stress tensor $\underset{\sim}{\boldsymbol{M}}$. The curl of the microdeformation rate is defined as

$$\operatorname{curl}\dot{\underset{\sim}{\hat{\boldsymbol{\chi}}}}^{p} := \epsilon_{jkl}\frac{\partial \dot{\hat{\chi}}^{p}_{ik}}{\partial x_l}\underline{\boldsymbol{e}}_i \otimes \underline{\boldsymbol{e}}_j = \dot{\underset{\sim}{\boldsymbol{K}}} \cdot \underset{\sim}{\boldsymbol{F}}^{-1} \tag{5}$$

The form of the power density of internal forces dictates the form of the power density of contact forces:

$$p^{(c)} = \underline{\boldsymbol{t}} \cdot \dot{\underline{\boldsymbol{u}}} + \underset{\sim}{\boldsymbol{m}} : \dot{\underset{\sim}{\hat{\boldsymbol{\chi}}}}^{p}, \quad \forall \underline{\boldsymbol{x}} \in \partial V \tag{6}$$

where $\underline{\boldsymbol{t}}$ is the usual simple traction vector and $\boldsymbol{m}$ the double traction tensor. The principle of virtual power is stated in the static case and in the absence of volume forces for the sake of brevity:

$$-\int_D p^{(i)}\,dV + \int_{\partial D} p^{(c)}\,dS = 0 \tag{7}$$

for all virtual fields $\dot{\underline{\boldsymbol{u}}}$, $\dot{\underset{\sim}{\hat{\boldsymbol{\chi}}}}^{p}$, and any subdomain $D \subset V$. By application of Gauss divergence theorem, assuming sufficient regularity of the fields, this statement expands into:

$$\int_V \frac{\partial \sigma_{ij}}{\partial x_j}\dot{u}_i\,dV + \int_V \left(\epsilon_{kjl}\frac{\partial M_{ik}}{\partial x_l} - s_{ij}\right)\dot{\hat{\chi}}^{p}_{ij}\,dV + \int_{\partial V}(t_i - \sigma_{ij}n_j)\dot{u}_i\,dS + \int_{\partial V}(m_{ik} - \epsilon_{jkl}M_{ij}n_l)\dot{\hat{\chi}}^{p}_{ik}\,dS = 0, \quad \forall \dot{u}_i,\ \forall \dot{\hat{\chi}}^{p}_{ij} \tag{8}$$

which leads to the two field equations of balance of momentum and generalized balance of moment of momentum, and two boundary conditions:

$$\operatorname{div}\underset{\sim}{\boldsymbol{\sigma}} = 0, \quad \operatorname{curl}\underset{\sim}{\boldsymbol{M}} + \underset{\sim}{\boldsymbol{s}} = 0, \quad \forall \underline{\boldsymbol{x}} \in V \tag{9}$$

$$\underline{\boldsymbol{t}} = \underset{\sim}{\boldsymbol{\sigma}} \cdot \underline{\boldsymbol{n}}, \quad \underset{\sim}{\boldsymbol{m}} = \underset{\sim}{\boldsymbol{M}} \cdot \underset{=}{\boldsymbol{\epsilon}} \cdot \underline{\boldsymbol{n}}, \quad \forall \underline{\boldsymbol{x}} \in \partial V \tag{10}$$

the index notation of the latter relation being $m_{ij} = M_{ik}\epsilon_{kjl}n_l$.

2.2. Constitutive equations

The deformation gradient is decomposed into elastic and plastic parts in the form

$$\underset{\sim}{\boldsymbol{F}} = \underset{\sim}{\boldsymbol{F}}^{e} \cdot \underset{\sim}{\boldsymbol{F}}^{p} \tag{11}$$

The isoclinic intermediate configuration is defined in a unique way by keeping the crystal orientation unchanged from the initial to the intermediate configuration following (Mandel, 1973). The plastic distortion $\boldsymbol{F}^p$ is invariant with respect to rigid body motions that are carried by $\boldsymbol{F}^e$. The current mass density is ρ whereas the mass density of the material element in the intermediate configuration is ρ_i, such that $\rho_i/\rho = J_e := \det \underset{\sim}{\boldsymbol{F}}^{e}$. The elastic strain is defined as

$$\underset{\sim}{\boldsymbol{E}}^{e} := \frac{1}{2}(\underset{\sim}{\boldsymbol{F}}^{eT} \cdot \underset{\sim}{\boldsymbol{F}}^{e} - \underset{\sim}{\mathbf{1}}) \tag{12}$$

The microdeformation is linked to the plastic deformation via the introduction of a relative deformation measure defined as

$$\underset{\sim}{\boldsymbol{e}}^{p} := \underset{\sim}{\boldsymbol{F}}^{p-1} \cdot \underset{\sim}{\hat{\boldsymbol{\chi}}}^{p} - \underset{\sim}{\mathbf{1}} \tag{13}$$

It measures the departure of the microdeformation from the plastic deformation, which will be associated with a cost in the free energy potential. When $\boldsymbol{e}^p \equiv 0$, the microdeformation coincides with the plastic deformation. The state variables are assumed to be the elastic strain, the relative deformation, the curl of microdeformation and some internal variables, α:

$$STATE := \left\{\underset{\sim}{\boldsymbol{E}}^{e}, \underset{\sim}{\boldsymbol{e}}^{p}, \underset{\sim}{\boldsymbol{K}}, \alpha\right\} \tag{14}$$

The specific Helmholtz free energy density, ψ, is assumed to be a function of this set of state variables. In particular, in this simple version of the model, the curl of microdeformation is assumed to contribute entirely to the stored energy. In more

sophisticated models, as proposed in Forest and Sievert (2006), Forest (2009) and Gurtin and Anand (2009), the relative deformation, the microdeformation and its gradient can be split into elastic and plastic parts. This is not necessary for the size effects to be described in the present work.

The dissipation rate density is the difference:

$$D := p^{(i)} - \rho\dot{\psi} \geqslant 0 \tag{15}$$

which must be positive according to the second principle of thermodynamics. When the previous strain measures are introduced, the power density of internal forces takes the following form:

$$\begin{aligned} p^{(i)} &= \underset{\sim}{\boldsymbol{\sigma}} : \dot{\underset{\sim}{\boldsymbol{F}}}^{e} \cdot \underset{\sim}{\boldsymbol{F}}^{e-1} + \underset{\sim}{\boldsymbol{\sigma}} : \underset{\sim}{\boldsymbol{F}}^{e} \cdot \dot{\underset{\sim}{\boldsymbol{F}}}^{p} \cdot \underset{\sim}{\boldsymbol{F}}^{p-1} \cdot \underset{\sim}{\boldsymbol{F}}^{e-1} + \underset{\sim}{\boldsymbol{s}} : (\underset{\sim}{\boldsymbol{F}}^{p} \cdot \dot{\underset{\sim}{\boldsymbol{e}}}^{p} + \dot{\underset{\sim}{\boldsymbol{F}}}^{p} \cdot \underset{\sim}{\boldsymbol{e}}^{p}) + \underset{\sim}{\boldsymbol{M}} : \dot{\underset{\sim}{\boldsymbol{K}}} \cdot \underset{\sim}{\boldsymbol{F}}^{-1} \\ &= \frac{\rho}{\rho_i} \underset{\sim}{\boldsymbol{\Pi}}^{e} : \dot{\underset{\sim}{\boldsymbol{E}}}^{e} + \frac{\rho}{\rho_i} \underset{\sim}{\boldsymbol{\Pi}}^{M} : \dot{\underset{\sim}{\boldsymbol{F}}}^{p} \cdot \underset{\sim}{\boldsymbol{F}}^{p-1} + \underset{\sim}{\boldsymbol{s}} : (\underset{\sim}{\boldsymbol{F}}^{p} \cdot \dot{\underset{\sim}{\boldsymbol{e}}}^{p} + \dot{\underset{\sim}{\boldsymbol{F}}}^{p} \cdot \underset{\sim}{\boldsymbol{e}}^{p}) + \underset{\sim}{\boldsymbol{M}} : \dot{\underset{\sim}{\boldsymbol{K}}} \cdot \underset{\sim}{\boldsymbol{F}}^{-1} \end{aligned} \tag{16}$$

where $\underset{\sim}{\boldsymbol{\Pi}}^{e}$ is the second Piola–Kirchhoff stress tensor with respect to the intermediate configuration and $\underset{\sim}{\boldsymbol{\Pi}}^{M}$ is the Mandel stress tensor:

$$\underset{\sim}{\boldsymbol{\Pi}}^{e} := J_e \underset{\sim}{\boldsymbol{F}}^{e-1} \cdot \underset{\sim}{\boldsymbol{\sigma}} \cdot \underset{\sim}{\boldsymbol{F}}^{e-T}, \quad \underset{\sim}{\boldsymbol{\Pi}}^{M} := J_e \underset{\sim}{\boldsymbol{F}}^{eT} \cdot \underset{\sim}{\boldsymbol{\sigma}} \cdot \underset{\sim}{\boldsymbol{F}}^{e-T} = \underset{\sim}{\boldsymbol{F}}^{eT} \cdot \underset{\sim}{\boldsymbol{F}}^{e} \cdot \underset{\sim}{\boldsymbol{\Pi}}^{e} \tag{17}$$

On the other hand,

$$\rho\dot{\psi} = \rho \frac{\partial \psi}{\partial \underset{\sim}{\boldsymbol{E}}^{e}} : \dot{\underset{\sim}{\boldsymbol{E}}}^{e} + \rho \frac{\partial \psi}{\partial \underset{\sim}{\boldsymbol{e}}^{p}} : \dot{\underset{\sim}{\boldsymbol{e}}}^{p} + \rho \frac{\partial \psi}{\partial \underset{\sim}{\boldsymbol{K}}} : \dot{\underset{\sim}{\boldsymbol{K}}} + \rho \frac{\partial \psi}{\partial \alpha} \dot{\alpha}$$

We compute

$$\begin{aligned} J_e D = &\left(\underset{\sim}{\boldsymbol{\Pi}}^{e} - \rho_i \frac{\partial \psi}{\partial \underset{\sim}{\boldsymbol{E}}^{e}} \right) : \dot{\underset{\sim}{\boldsymbol{E}}}^{e} + \left(J_e \underset{\sim}{\boldsymbol{F}}^{pT} \cdot \underset{\sim}{\boldsymbol{s}} - \rho_i \frac{\partial \psi}{\partial \underset{\sim}{\boldsymbol{e}}^{p}} \right) : \dot{\underset{\sim}{\boldsymbol{e}}}^{p} + \left(J_e \underset{\sim}{\boldsymbol{M}} \cdot \underset{\sim}{\boldsymbol{F}}^{-T} - \rho_i \frac{\partial \psi}{\partial \underset{\sim}{\boldsymbol{K}}} \right) : \dot{\underset{\sim}{\boldsymbol{K}}} \\ &+ \left(\underset{\sim}{\boldsymbol{\Pi}}^{M} + J_e \underset{\sim}{\boldsymbol{s}} \cdot \underset{\sim}{\hat{\boldsymbol{\chi}}}^{pT} \right) : \dot{\underset{\sim}{\boldsymbol{F}}}^{p} \cdot \underset{\sim}{\boldsymbol{F}}^{p-1} - \rho_i \frac{\partial \psi}{\partial \alpha} \dot{\alpha} \geqslant 0 \end{aligned} \tag{18}$$

Assuming that the processes associated with $\dot{\underset{\sim}{\boldsymbol{E}}}^{e}$, $\dot{\underset{\sim}{\boldsymbol{e}}}^{p}$ and $\dot{\underset{\sim}{\boldsymbol{K}}}$ are non-dissipative, the state laws are obtained:

$$\underset{\sim}{\boldsymbol{\Pi}}^{e} = \rho_i \frac{\partial \psi}{\partial \underset{\sim}{\boldsymbol{E}}^{e}}, \quad \underset{\sim}{\boldsymbol{s}} = J_e^{-1} \underset{\sim}{\boldsymbol{F}}^{p-T} \cdot \rho_i \frac{\partial \psi}{\partial \underset{\sim}{\boldsymbol{e}}^{p}}, \quad \underset{\sim}{\boldsymbol{M}} = J_e^{-1} \rho_i \frac{\partial \psi}{\partial \underset{\sim}{\boldsymbol{K}}} \cdot \underset{\sim}{\boldsymbol{F}}^{T} \tag{19}$$

The residual dissipation rate is

$$J_e D = \left(\underset{\sim}{\boldsymbol{\Pi}}^{M} + J_e \underset{\sim}{\boldsymbol{s}} \cdot \underset{\sim}{\hat{\boldsymbol{\chi}}}^{pT} \right) : \dot{\underset{\sim}{\boldsymbol{F}}}^{p} \cdot \underset{\sim}{\boldsymbol{F}}^{p-1} - R\dot{\alpha} \geqslant 0, \quad \text{with } R := \rho_i \frac{\partial \psi}{\partial \alpha} \tag{20}$$

At this stage, a dissipation potential, function of stress measures, $\Omega(\underset{\sim}{\mathscr{S}}, R)$, is introduced in order to formulate the evolution equations for plastic flow and internal variables:

$$\dot{\underset{\sim}{\boldsymbol{F}}}^{p} \cdot \underset{\sim}{\boldsymbol{F}}^{p-1} = \frac{\partial \Omega}{\partial \underset{\sim}{\mathscr{S}}}, \quad \text{with } \underset{\sim}{\mathscr{S}} := \underset{\sim}{\boldsymbol{\Pi}}^{M} + J_e \underset{\sim}{\boldsymbol{s}} \cdot \underset{\sim}{\hat{\boldsymbol{\chi}}}^{pT}, \quad \dot{\alpha} = -\frac{\partial \Omega}{\partial R} \tag{21}$$

where R is the thermodynamic force associated with the internal variable α, and $\underset{\sim}{\mathscr{S}}$ is the effective stress conjugate to plastic strain rate, the driving force for plastic flow.

In the case of crystal plasticity, a generalized Schmid law is adopted for each slip system s in the form:

$$f^s(\underset{\sim}{\mathscr{S}}, \tau_c^s) = |\underset{\sim}{\mathscr{S}} : \underset{\sim}{\boldsymbol{P}}^s| - \tau_c^s \geqslant 0, \quad \text{with } \underset{\sim}{\boldsymbol{P}}^s = \underline{\boldsymbol{l}}^s \otimes \underline{\boldsymbol{n}}^s \tag{22}$$

for activation of slip system s with slip direction, $\underline{\boldsymbol{l}}^s$, and normal to the slip plane, $\underline{\boldsymbol{n}}^s$. We call $\underset{\sim}{\boldsymbol{P}}^s$ the orientation tensor. The critical resolved shear stress is τ_c^s which may be a function of R in the presence of isotropic hardening. The kinematics of plastic slip follows from the choice of a dissipation potential, $\Omega(f^s)$, that depends on the stress variables through the yield function itself, f^s:

$$\dot{\underset{\sim}{\boldsymbol{F}}}^{p} \cdot \underset{\sim}{\boldsymbol{F}}^{p-1} = \sum_{s=1}^{N} \frac{\partial \Omega}{\partial f^s} \frac{\partial f^s}{\partial \underset{\sim}{\mathscr{S}}} = \sum_{s=1}^{N} \dot{\gamma}^s \underset{\sim}{\boldsymbol{P}}^s, \quad \text{with } \dot{\gamma}^s = \frac{\partial \Omega}{\partial f^s} \operatorname{sign}(\underset{\sim}{\mathscr{S}} : \underset{\sim}{\boldsymbol{P}}^s) \tag{23}$$

A possible viscoplastic potential is then:

$$\Omega(f^s) = \frac{K}{n+1} \left\langle \frac{f^s}{K} \right\rangle^{n+1},$$

where K, n are viscosity parameters associated with viscoplastic slip, and the brackets stand for $\langle \cdot \rangle = Max\,(0, \cdot)$. The generalized resolved shear stress can be decomposed into two contributions:

$$\underset{\sim}{\mathscr{S}} : \underset{\sim}{\boldsymbol{P}}^s = \tau^s - x^s, \quad \text{with } \tau^s = \underset{\sim}{\boldsymbol{\Pi}}^{M} : \underset{\sim}{\boldsymbol{P}}^s \quad \text{and} \quad x^s = -\underset{\sim}{\boldsymbol{s}} \cdot \underset{\sim}{\hat{\boldsymbol{\chi}}}^{pT} : \underset{\sim}{\boldsymbol{P}}^s \tag{24}$$

The usual resolved shear stress is τ^s whereas x^s can be interpreted as an internal stress or back-stress leading to kinematic hardening. The fact that the introduction of the effect of the dislocation density tensor or, more generally, of gradient of plastic strain tensor, leads to the existence of internal stresses induced by higher order stresses has already been noticed by Steinmann (1996) (see also Forest, 2008). The back-stress component is induced by the microstress $\underset{\sim}{\boldsymbol{s}}$ or, equivalently, by the curl of the generalized couple stress tensor, $\boldsymbol{M}$, via the balance Eq. (9).

When deformations and rotations remain sufficiently small, the previous equations can be linearized as follows:

$$\underset{\sim}{\boldsymbol{F}} = \underset{\sim}{\mathbf{1}} + \underset{\sim}{\boldsymbol{H}} \simeq \underset{\sim}{\mathbf{1}} + \underset{\sim}{\boldsymbol{H}}^e + \underset{\sim}{\boldsymbol{H}}^p, \quad \underset{\sim}{\boldsymbol{H}}^e = \underset{\sim}{\boldsymbol{\varepsilon}}^e + \underset{\sim}{\omega}^e, \quad \underset{\sim}{\boldsymbol{H}}^p = \underset{\sim}{\boldsymbol{\varepsilon}}^p + \underset{\sim}{\omega}^p \tag{25}$$

where $\boldsymbol{\varepsilon}^e$, $\boldsymbol{\omega}^e$ (resp. $\boldsymbol{\varepsilon}^p$, $\boldsymbol{\omega}^p$) are the symmetric and skew-symmetric parts of $\boldsymbol{F}^e - \mathbf{1}$ (resp. $\boldsymbol{F}^p - \mathbf{1}$). When microdeformation is small, the relative deformation is linearized as

$$\underset{\sim}{\boldsymbol{e}}^p = (\underset{\sim}{\mathbf{1}} + \underset{\sim}{\boldsymbol{H}}^p)^{-1} \cdot (\underset{\sim}{\mathbf{1}} + \underset{\sim}{\boldsymbol{\chi}}^p) - \underset{\sim}{\mathbf{1}} \simeq \underset{\sim}{\boldsymbol{\chi}}^p - \underset{\sim}{\boldsymbol{H}}^p, \quad \text{with } \underset{\sim}{\boldsymbol{\chi}}^p = \underset{\sim}{\hat{\boldsymbol{\chi}}}^p - \underset{\sim}{\mathbf{1}} \tag{26}$$

When linearized, the state laws (19) become:

$$\underset{\sim}{\boldsymbol{\sigma}} = \rho \frac{\partial \psi}{\partial \underset{\sim}{\boldsymbol{\varepsilon}}^e}, \ \underset{\sim}{\boldsymbol{s}} = \rho \frac{\partial \psi}{\partial \underset{\sim}{\boldsymbol{e}}^p}, \ \underset{\sim}{\boldsymbol{M}} = \rho \frac{\partial \psi}{\partial \underset{\sim}{\boldsymbol{K}}}.$$

The evolution equations read then:

$$\underset{\sim}{\dot{\boldsymbol{\varepsilon}}}^p = \frac{\partial \Omega}{\partial (\underset{\sim}{\boldsymbol{\sigma}} + \underset{\sim}{\boldsymbol{s}})}, \ \dot{\alpha} = -\frac{\partial \Omega}{\partial R}.$$

We adopt the most simple case of a quadratic free energy potential:

$$\rho\psi(\underset{\sim}{\boldsymbol{\varepsilon}}^e, \underset{\sim}{\boldsymbol{e}}^p, \underset{\sim}{\boldsymbol{K}}) = \frac{1}{2} \underset{\sim}{\boldsymbol{\varepsilon}}^e : \underset{\approx}{\boldsymbol{C}} : \underset{\sim}{\boldsymbol{\varepsilon}}^e + \frac{1}{2} H_\chi \underset{\sim}{\boldsymbol{e}}^p : \underset{\sim}{\boldsymbol{e}}^p + \frac{1}{2} A \underset{\sim}{\boldsymbol{K}} : \underset{\sim}{\boldsymbol{K}} \tag{27}$$

The usual four-rank tensor of elastic moduli is denoted by $\boldsymbol{C}$. The higher order moduli have been limited to only two additional parameters: H_χ (unit MPa) and A (unit MPa mm^2). Their essential impact on the prediction of size effect will be analyzed in the next section. It follows that

$$\underset{\sim}{\boldsymbol{\sigma}} = \underset{\approx}{\boldsymbol{C}} : \underset{\sim}{\boldsymbol{\varepsilon}}^e, \quad \underset{\sim}{\boldsymbol{s}} = H_\chi \underset{\sim}{\boldsymbol{e}}^p, \quad \underset{\sim}{\boldsymbol{M}} = A \underset{\sim}{\boldsymbol{K}} \tag{28}$$

Large values of H_χ ensure that $\boldsymbol{e}^p$ remains small so that $\hat{\boldsymbol{\chi}}^p$ remains close to $\boldsymbol{H}^p$ and $\boldsymbol{K}$ is close to the dislocation density tensor. The yield condition for each slip system becomes

$$f^s = |\tau^s - x^s| - \tau_c^s, \quad \text{with } x^s = -\underset{\sim}{\boldsymbol{s}} : \underset{\sim}{\boldsymbol{P}}^s = (\operatorname{curl} \underset{\sim}{\boldsymbol{M}}) : \underset{\sim}{\boldsymbol{P}}^s = A(\operatorname{curl}\operatorname{curl} \underset{\sim}{\boldsymbol{\chi}}^p) : \underset{\sim}{\boldsymbol{P}}^s \tag{29}$$

2.3. Size effects in a two-phase single crystal laminate

Let us consider a periodic two-phase single crystal laminate under simple shear as in Forest (2008) and Cordero et al. (2010). This microstructure is described in Fig. 1; it is composed of a hard elastic phase (h) and a soft elasto-plastic phase (s) where one slip system with slip direction normal to the interface between (h) and (s) is considered. A mean simple glide $\bar{\gamma}$ is applied in the crystal slip direction of the phase (s). We consider a displacement and microdeformation fields of the form:

$$u_1 = \bar{\gamma} x_2, \quad u_2(x_1), \quad u_3 = 0, \quad \chi^p_{12}(x_1), \quad \chi^p_{21}(x_1) \tag{30}$$

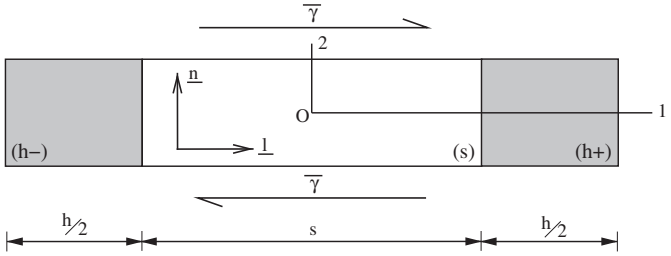

Fig. 1. Single slip in a periodic two-phase single crystal laminate under simple shear: the gray phase (h) displays a purely linear elastic behavior whereas the inelastic deformation of the white elasto-plastic phase (s) is controlled by a single slip system ($\underline{\boldsymbol{n}}, \underline{\boldsymbol{l}}$).

within the context of small deformation theory. It follows that

$$[\underset{\sim}{\boldsymbol{H}}] = \begin{bmatrix} 0 & \bar{\gamma} & 0 \\ u_{2,1} & 0 & 0 \\ 0 & 0 & 0 \end{bmatrix} \quad [\underset{\sim}{\boldsymbol{H}^p}] = \begin{bmatrix} 0 & \gamma & 0 \\ 0 & 0 & 0 \\ 0 & 0 & 0 \end{bmatrix} \quad [\underset{\sim}{\boldsymbol{H}^e}] = \begin{bmatrix} 0 & \bar{\gamma}-\gamma & 0 \\ u_{2,1} & 0 & 0 \\ 0 & 0 & 0 \end{bmatrix} \tag{31}$$

$$[\underset{\sim}{\boldsymbol{\chi}^p}] = \begin{bmatrix} 0 & \chi^p_{12}(x_1) & 0 \\ \chi^p_{21}(x_1) & 0 & 0 \\ 0 & 0 & 0 \end{bmatrix} \quad [\operatorname{curl}\underset{\sim}{\boldsymbol{\chi}^p}] = \begin{bmatrix} 0 & 0 & -\chi^p_{12,1} \\ 0 & 0 & 0 \\ 0 & 0 & 0 \end{bmatrix} \tag{32}$$

The resulting stress tensors are

$$[\underset{\sim}{\boldsymbol{\sigma}}] = \mu \begin{bmatrix} 0 & \bar{\gamma}-\gamma+u_{2,1} & 0 \\ \bar{\gamma}-\gamma+u_{2,1} & 0 & 0 \\ 0 & 0 & 0 \end{bmatrix} \quad [\underset{\sim}{\boldsymbol{s}}] = -H_\chi \begin{bmatrix} 0 & \gamma-\chi^p_{12} & 0 \\ -\chi^p_{21} & 0 & 0 \\ 0 & 0 & 0 \end{bmatrix} \tag{33}$$

$$[\underset{\sim}{\boldsymbol{M}}] = \begin{bmatrix} 0 & 0 & -A\chi^p_{12,1} \\ 0 & 0 & 0 \\ 0 & 0 & 0 \end{bmatrix} \quad [\operatorname{curl}\underset{\sim}{\boldsymbol{M}}] = \begin{bmatrix} 0 & -A\chi^p_{12,11} & 0 \\ 0 & 0 & 0 \\ 0 & 0 & 0 \end{bmatrix} \tag{34}$$

These forms of matrices are valid for both phases, except that $\gamma \equiv 0$ in the hard elastic phase. Each phase possesses its own material parameters, H_χ and A, the shear modulus, μ, being assumed for simplicity to be identical in both phases. The balance equation, $\underset{\sim}{\boldsymbol{s}} = -\operatorname{curl}\underset{\sim}{\boldsymbol{M}}$, gives $\chi^p_{21} = 0$ and the plastic slip:

$$\gamma = \chi^p_{12} - \frac{A}{H_\chi}\chi^p_{12,11} \tag{35}$$

In the soft phase, the plasticity criterion stipulates that

$$\sigma_{12} + s_{12} = \tau_c + H\gamma_{cum} \tag{36}$$

where H is a linear hardening modulus considered in this phase and γ_{cum} is the cumulative plastic slip defined by $\dot{\gamma}_{cum} = |\dot{\gamma}|$. The following analytical resolution is done for the first loading branch, under monotonic loading. The slip direction, $\underline{\boldsymbol{I}}$, has been chosen such that $\gamma > 0$ for this first loading branch, so that we have $\gamma_{cum} = \gamma$. Considering Eqs. (35) and (36), we obtain the second order differential equation for the microdeformation variable in the soft phase, χ^{ps}_{12},

$$\frac{1}{\omega^{s2}}\chi^{ps}_{12,11} - \chi^{ps}_{12} = \frac{\tau_c - \sigma_{12}}{H}, \quad \text{with } \omega^s = \sqrt{\frac{H^s_\chi H}{A^s\left(H^s_\chi + H\right)}} \tag{37}$$

where $1/\omega^s$ is the characteristic length of the soft phase for this boundary value problem. The force stress balance equation requires σ_{12} to be uniform. It follows that the non-homogeneous part of the differential equation is constant and then the hyperbolic profile of χ^{ps}_{12} takes the form:

$$\chi^{ps}_{12} = C^s \cosh(\omega^s x) + D \tag{38}$$

where C^s and D are constants to be determined. Symmetry conditions ($\chi^{ps}_{12}(-s/2) = \chi^{ps}_{12}(s/2)$) have been taken into account.

In the elastic phase, where the plastic slip vanishes, an hyperbolic profile of the microdeformation variable, χ^{ph}_{12}, is also obtained:

$$\chi^{ph}_{12} = C^h \cosh\left(\omega^h\left(x \pm \frac{s+h}{2}\right)\right), \quad \text{with } \omega^h = \sqrt{\frac{H^h_\chi}{A^h}} \tag{39}$$

where, again, C^h is a constant to be determined. It is remarkable that the plastic microvariable, χ^{ph}_{12}, does not vanish in the elastic phase, close to the interfaces, although no plastic deformation takes place. This is due to the transmission of double traction. Such a transmission has been shown in Cordero et al. (2010) to be essential for size effects to occur. The meaning of the linear constitutive equation for the double stress tensor in (28) can be interpreted, for the elastic phase, as non-local elasticity. That is why the corresponding characteristic length, $1/\omega^h$, will be kept of the order of nanometer in the presented simulation.

The coefficients C^s, D and C^h can be identified using the interface and periodicity conditions:

- Continuity of χ^p_{12} at $x = \pm s/2$:

$$C^s \cosh\left(\omega^s \frac{s}{2}\right) + D = C^h \cosh\left(\omega^h \frac{h}{2}\right)$$

- Continuity of the double traction, as given in Eq. (10), $m_{12} = -M_{13}$ at $x = \pm s/2$:

$$A^s\omega^s C^s \sinh\left(\omega^s \frac{s}{2}\right) = -A^h\omega^h C^h \sinh\left(\omega^h \frac{h}{2}\right). \tag{40}$$

- Periodicity of displacement component u_2. The constant stress component $\sigma_{12} = \mu(\bar{\gamma} - \gamma + u_{2,1})$ is obtained from the plasticity criterion in the soft phase (Eq. (36)):

$$\sigma_{12} = \tau_c + H\gamma_{cum} - A^s\chi^{ps}_{12,11} \tag{41}$$

Still considering the first loading branch for which $\gamma_{cum} = \gamma$, it follows that

$$u^s_{2,1} = \frac{\sigma_{12}}{\mu} - \bar{\gamma} + \gamma = \frac{\tau_c}{\mu} - \bar{\gamma} + \frac{A^s\omega^{s2}C^s}{H}\cosh(\omega^s x) + \frac{H+\mu}{\mu}D \tag{42}$$

in the soft phase and $u^h_{2,1} = \frac{\sigma_{12}}{\mu} - \bar{\gamma} = \frac{\tau_c}{\mu} - \bar{\gamma} + \frac{H}{\mu}D$, in the hard phase. The average on the whole structure,

$$\int_{-(s+h)/2}^{(s+h)/2} u_{2,1}\,dx = 0 \tag{43}$$

must vanish for periodicity reasons and gives

$$\left(\frac{\tau_c}{\mu} - \bar{\gamma}\right)(s+h) + \frac{2A^s\omega^s C^s}{H}\sinh\left(\omega^s\frac{s}{2}\right) + \frac{H(s+h)+\mu s}{\mu}D = 0 \tag{44}$$

Fig. 2 shows the profiles of plastic microdeformation in the two-phase laminate for different sets of material parameters and for a fraction of soft phase (s), $f_s = 0.7$. These profiles clearly show the continuity of χ^p_{12} at the interfaces. The different shapes presented are obtained for various values of the modulus A^s, the other material parameters being fixed and given in Table 1. When the intrinsic length scale is small compared to the size of the microstructure, the microdeformation gradient can develop inside the phase (s) which leads to a rounded profile of the plastic microdeformation χ^{ps}_{12}. When the intrinsic length scale becomes of the order of the size of the microstructure or even larger, the model starts to saturate so that χ^{ps}_{12} becomes quasi-homogeneous (flat profile).

From Eq. (41) we derive the expression of the macroscopic stress tensor component, Σ_{12}, defined as the mean value of the stress component σ_{12} over the microstructure size, $l = (s + h)$:

$$\Sigma_{12} = \langle\sigma_{12}\rangle = \frac{1}{l}\int_{-\frac{l}{2}}^{\frac{l}{2}}\sigma_{12}\,dx = \tau_c + \frac{H}{f_s}\langle\gamma^{cum}\rangle - \frac{A^s}{f_s}\langle\chi^{ps}_{12,11}\rangle, \tag{45}$$

where brackets $\langle\cdot\rangle$ denote the average values over the microstructure unit cell.

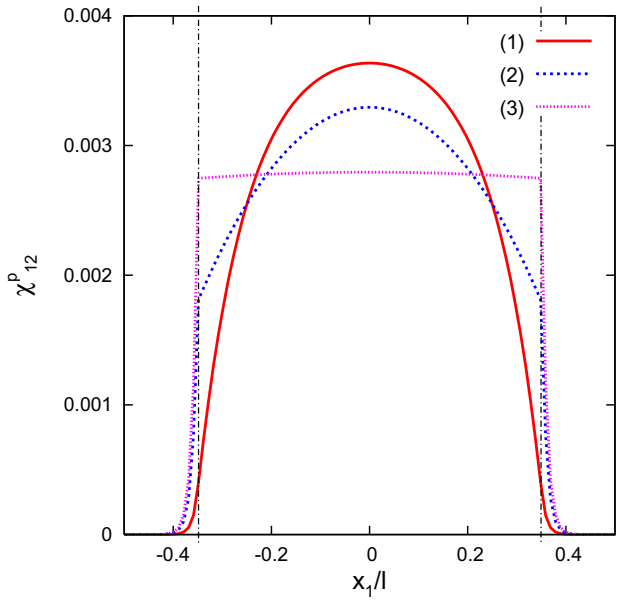

Fig. 2. Profiles of plastic microdeformation χ^p_{12} in the two-phase microstructure with the *microcurl* model at 0.2% overall plastic strain obtained with the set of material parameters given in Table 1 and (1) in the absence of mismatch between the moduli of the two phases, $A^h = A^s = 5 \times 10^{-5}$ MPa mm^2, (2) with a stronger mismatch, $A^h = 5 \times 10^{-5}$ MPa mm^2 and $A^s = 1 \times 10^{-3}$ MPa mm^2 and (3) $A^h = 5 \times 10^{-5}$ MPa mm^2 and $A^s = 5 \times 10^{-2}$ MPa mm^2. The associated intrinsic length scales, $1/\omega^s$, are respectively: 100 nm, 449 nm and 3.2 μm. In all three cases, the fraction of soft phase $f_s = 0.7$ and the microstructure size is fixed, $l = 1$ μm. The vertical lines indicate the position of interfaces.

Table 1
Set of material parameters used in the simulations. The intrinsic length scales, defined as $1/\omega^{h,s}$, induced by these parameters is of the order of 10 nm for the elastic phase (h) and 500 nm for the plastic phase (s).

	μ [MPa]	τ_c [MPa]	H [MPa]	H_χ [MPa]	A [MPa mm^2]
Phase (s)	35000	40	5000	500000	1×10^{-3}
Phase (h)	35000	–	–	500000	5×10^{-5}

We obtain the mean plastic slip for the first loading branch from Eq. (35):

$$\langle\gamma\rangle = \left\langle \chi^{ps}_{12} - \frac{A^s}{H^s_\chi}\chi^{ps}_{12,11}\right\rangle = \frac{2A^s\omega^s C^s \sinh\left(\omega^s\frac{f_s l}{2}\right)}{Hl} + f_s D, \tag{46}$$

where f_s is the fraction of soft phase. From this we obtain expressions of C^s and D as functions of $\langle\gamma\rangle$,

$$C^s = -\langle\gamma\rangle\left[A^s\omega^s\sinh\left(\omega^s\frac{f_s l}{2}\right)\left(f_s\left(\frac{\coth\left(\omega^s\frac{f_s l}{2}\right)}{A^s\omega^s}+\frac{\coth\left(\omega^h\frac{(1-f_s)l}{2}\right)}{A^h\omega^h}\right)-\frac{2}{Hl}\right)\right]^{-1} \tag{47}$$

$$D = \langle\gamma\rangle\left[f_s - \frac{2}{Hl}\left(\frac{\coth\left(\omega^s\frac{f_s l}{2}\right)}{A^s\omega^s}+\frac{\coth\left(\omega^h\frac{(1-f_s)l}{2}\right)}{A^h\omega^h}\right)^{-1}\right]^{-1} \tag{48}$$

The macroscopic stress takes the form:

$$\Sigma_{12} = \tau_c + HD\langle\gamma\rangle \tag{49}$$

The hardening produced by the model is a combination of the kinematic hardening arising from the higher order back-stress component and the linear isotropic hardening introduced in (36). Its modulus, H^{tot}, is size-dependent and is obtained using Eqs. (48) and (49):

$$H^{tot} = H\left[f_s - \frac{2}{Hl}\left(\frac{\coth\left(\omega^s\frac{f_s l}{2}\right)}{A^s\omega^s}+\frac{\coth\left(\omega^h\frac{(1-f_s)l}{2}\right)}{A^h\omega^h}\right)^{-1}\right]^{-1} \tag{50}$$

When the size of the elasto-plastic phase (s) becomes large compared to the intrinsic length scale $1/\omega_s$, strain gradient effect is small and the kinematic hardening arising from the *microcurl* model tends to vanish. Then the model reduces to conventional crystal plasticity theory. In contrast, the maximum extra-stress, $\Delta\Sigma$, predicted by the model at small microstructure sizes can be computed as

$$\Delta\Sigma = \lim_{l\to 0}\Sigma_{12}(\langle\gamma\rangle) - \lim_{l\to\infty}\Sigma_{12|0.2} = \frac{1-f_s}{f_s}H_\chi\langle\gamma\rangle \tag{51}$$

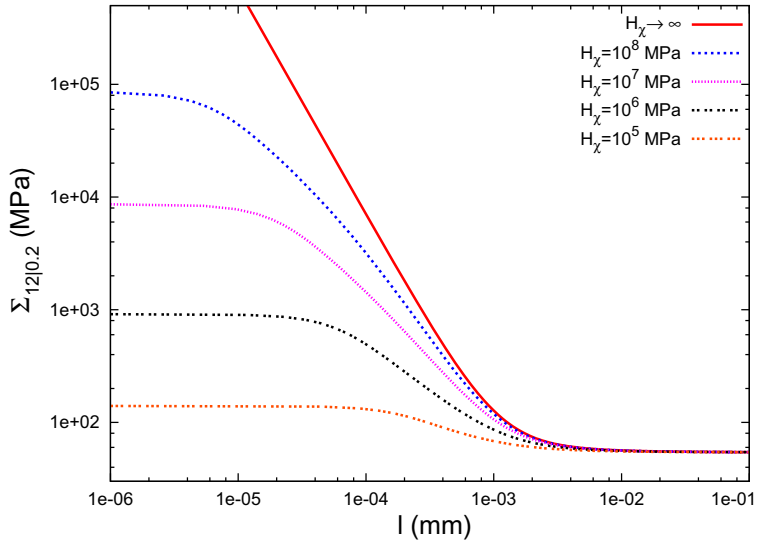

Fig. 3. Evolution of the macroscopic flow stress $\Sigma_{12|0.2}$ at 0.2% plastic strain as a function of the microstructure length scale l, plotted for different coupling moduli $H_\chi(=H^s_\chi=H^h_\chi)$. The other material parameters are given in Table 1 and $f_s=0.7$.

Fig. 3 presents the predicted evolution of the macroscopic flow stress $\Sigma_{12|0.2}$ at 0.2% plastic strain (obtained by setting $\langle\gamma\rangle = 0.002$) as a function of the microstructure length scale l in a log–log diagram. This evolution is plotted using the material parameters given in Table 1 and for various values of the coupling modulus, $H^s_\chi = H^h_\chi = H_\chi$. The four lower curves exhibit a *tanh*-shape with saturation for large ($l > 10^{-2}$ mm) and small ($l < 10^{-5}$ mm) values of l. A transition domain with strong size dependence is observed between these two plateaus. The limits and the maximum extra-stress, the position of the transition zone and the scaling law exponent in the size dependent domain (defined as the slope in the log–log diagram) are directly related to the material parameters used in the model. The *microcurl* model can produce scaling law exponents ranging from 0 to −2. The upper curve is obtained for $H_\chi \to \infty$, it no longer exhibits a *tanh*-shape as no saturation occurs for small values of l, the limit $\Delta\Sigma \to \infty$ follows. This limit case will be described in next subsection.

2.4. Strain gradient plasticity as a limit case

In the proposed *microcurl* model, the modulus H_χ introduces a coupling between micro and macro variables. A high value of H_χ forces the plastic microdeformation $\boldsymbol{\chi}^p$ to remain as close as possible to the macro plastic deformation $\boldsymbol{H}^p$. Consequently, it enforces the condition that $\boldsymbol{K}$ cõincides with the dislocation density tensor. In this case, the *microc̃url* model degenerates into the strain gradient plas̃ticity model by Gurtin (2002). The *microcurl* model can then be used to predict the response of the strain gradient plasticity model in the size effect zone. For that purpose, let us consider the limit of $\Sigma_{12|0.2}$, when H_χ goes to infinity. Indeed, when H_χ tends to infinity, the expression of D in Eq. (48) can be simplified. We consider sizes of the microstructures in the size effect zone, i.e. intermediate values of l. Since H_χ is very high, the term $\tanh(\omega^h(1-f_s)l/2)$ tends to 1. Considering that l is small enough, the term $l\,(tanh(\omega_s f_s l/2))$ can be approximated by its Taylor expansion at the order 2, which leads to D of the form:

$$D \approx \frac{al+b}{cl^2+dl+e} \tag{52}$$

$$a = \frac{\langle\gamma\rangle f_s}{2\sqrt{H_\chi}}, \quad b = \langle\gamma\rangle f_s A^h\left(1+\frac{H}{H_\chi}\right), \quad c = -\frac{f_s^3 H\sqrt{A^h}}{12}, \quad d = \frac{f_s^2 H}{2\sqrt{H_\chi}}, \quad e = -\frac{f_s\sqrt{A^h}H}{H_\chi} \tag{53}$$

The terms a, d and e tend to 0 when $H_\chi \to \infty$, so that

$$D \approx \frac{12A_s\langle\gamma\rangle}{f_s^3 H l^2},$$

and the macroscopic stress is

$$\Sigma_{12} \approx \tau_c + \frac{12A_s\langle\gamma\rangle}{f_s^3 l^2} \tag{54}$$

This expression indicates a l^{-2} scaling law for the strain gradient plasticity model. This scaling law differs from Hall–Petch relation, $l^{-1/2}$, typical for grain size effects, and from Orowan's law, l^{-1}, valid for precipitate size effects.

3. Microdamage modeling of cracking in single crystals

Cracks in single crystals occur on specific cleavage planes in brittle crystals with BCC and HCP structures (Parisot et al., 2004). In ductile single crystals like aluminum, copper or even nickel base superalloys (Flouriot et al., 2003), cracking is also observed in specific crystallographic planes following intense shear activity in some slip planes, under monotonic or cyclic loading conditions. These observations prompted (Musienko & Cailletaud, 2009) to formulate a single crystal plasticity and damage model that attributes damage variables to specific crystallographic planes in order to simulate crack propagation in the individual grains of a polycrystal. A regularization procedure based on the micromorphic continuum has then been proposed in Aslan and Forest (2009) to limit the mesh-dependency of the results of such finite element simulations. The damage variables introduced in these models are defined as irreversible strains that measure the apparent deformation of the micro-cracked volume element. Such strain-based damaged models differ from classical brittle damage mechanics theories where a damage variable is introduced that varies from 0 to 1 and that rely on the degradation of the elastic stiffness. They are more closely related to ductile models of fracture accounting for cavity initiation and growth, see (Besson, 2009). The model presented in this section introduces several crystallographic damage mechanisms in the spirit of multi-mechanism plasticity and damage theory (Besson, 2009). This represents a similar choice of variable as the equivalent strain measure used in the gradient damage models by Peerlings, Massart, and Geers (2004), for the mesh-independent simulation of crack propagation in isotropic materials.

3.1. Balance equations

Microdamage theory restricts the gradient effect to a scalar damage variable d, the precise definition of which will be given later. The number of additional degrees of freedom is deliberately limited to a single one with a view to efficient

numerical simulations of crack propagation which are quite demanding from the computational point of view. Therefore, the degrees of freedom are the vector component u_i and the scalar microdamage variable ${}^{\chi}d$. The degrees of freedom and their gradients on which constitutive relations may depend, are as follows:

$$DOF = \{\underline{\boldsymbol{u}}, {}^{\chi}d\}, \quad GRAD = \left\{\underset{\sim}{\boldsymbol{F}} := \underset{\sim}{\mathbf{1}} + \underline{\boldsymbol{u}} \otimes \boldsymbol{\nabla}_X, \boldsymbol{\nabla}_X {}^{\chi}d\right\} \tag{55}$$

In order to derive the balance and boundary conditions, the method of virtual power is used and power of internal forces are written as

$$p^{(i)} = \underset{\sim}{\boldsymbol{\sigma}} : (\dot{\underline{\boldsymbol{u}}} \otimes \boldsymbol{\nabla}_x) + a\dot{{}^{\chi}d} + \underline{\boldsymbol{b}} \cdot \boldsymbol{\nabla}_x \dot{{}^{\chi}d}, \quad \forall \underline{\boldsymbol{x}} \in V \tag{56}$$

where a and $\underline{\boldsymbol{b}}$ are generalized stresses. Note that, in this expression, the gradients of velocity fields are taken with respect to the current coordinates. Corresponding power density of contact forces reads:

$$p^{(c)} = \underline{\boldsymbol{t}} \cdot \dot{\underline{\boldsymbol{u}}} + a_c \dot{{}^{\chi}d}, \quad \forall \underline{\boldsymbol{x}} \in \partial V \tag{57}$$

where $\underline{\boldsymbol{t}}$ is the traction vector and a_c is the generalized traction. The variational formulation of the static microdamage problem can be derived directly from the principle of virtual power as

$$-\int_{\Omega} (\underset{\sim}{\boldsymbol{\sigma}} : \dot{\underset{\sim}{\boldsymbol{F}}} \cdot \underset{\sim}{\boldsymbol{F}}^{-1} + a\dot{{}^{\chi}d} + \underline{\boldsymbol{b}} \cdot \nabla \dot{{}^{\chi}d}) dV + \int_{\partial\Omega} (\underline{\boldsymbol{t}} \cdot \dot{\underline{\boldsymbol{u}}} + a_c \dot{{}^{\chi}d}) dS = 0 \tag{58}$$

from which momentum and generalized balance equations are derived by using Gauss divergence theorem, together with the associated boundary conditions:

$$\operatorname{div} \underset{\sim}{\boldsymbol{\sigma}} = 0, \quad a = \operatorname{div} \underset{\sim}{\boldsymbol{b}}, \quad \forall \underline{\boldsymbol{x}} \in V \tag{59}$$

$$\underline{\boldsymbol{t}} = \underset{\sim}{\boldsymbol{\sigma}} \cdot \underline{\boldsymbol{n}}, \quad a_c = \underline{\boldsymbol{b}} \cdot \underline{\boldsymbol{n}}, \quad \forall \underline{\boldsymbol{x}} \in \partial V \tag{60}$$

3.2. Constitutive coupling between plasticity and damage for single crystals

We consider plasticity and damage as inelastic deformation mechanisms so that the deformation gradient is decomposed into elastic and inelastic parts:

$$\underset{\sim}{\boldsymbol{F}} = \underset{\sim}{\boldsymbol{F}}^{e} \cdot \underset{\sim}{\boldsymbol{F}}^{i} \tag{61}$$

Note that the orientation of the intermediate configuration is such that the lattice vectors do not rotate from the initial to the intermediate configuration. Such a definition is possible only if both the plasticity and damage mechanisms have common crystallographic features. In particular, crystallographic fracture planes will be chosen so that the crystal orientation will not be affected by the development of damage from the initial to the intermediate isoclinic configuration. The plastic strain rate $\dot{\boldsymbol{F}}^{i} \cdot \boldsymbol{F}^{i-1}$ is not expected to be traceless since it will contain a damage part. Accordingly, the volume change associated with inelastic phenomena is $J_i = \det \boldsymbol{F}^{i} \neq 1$ in the presence of damage. The elastic strain measure is still defined by Eq. (12). Elastic strain, microdamage, the gradient of microdamage and α, referring to any other internal variable, are considered as the state variables:

$$STATE := \left\{\underset{\sim}{\boldsymbol{E}}^{e}, {}^{\chi}d, \boldsymbol{\nabla}_X {}^{\chi}d, \alpha\right\} \tag{62}$$

$$\rho_i \dot{\psi} = \rho_i \frac{\partial \psi}{\partial \underset{\sim}{\boldsymbol{E}}^{e}} : \dot{\underset{\sim}{\boldsymbol{E}}}^{e} + \rho_i \frac{\partial \psi}{\partial {}^{\chi}d} \dot{{}^{\chi}d} + \rho_i \frac{\partial \psi}{\partial \boldsymbol{\nabla}_X {}^{\chi}d} \cdot \boldsymbol{\nabla}_X \dot{{}^{\chi}d} + \rho_i \frac{\partial \psi}{\partial \alpha} \dot{\alpha}, \tag{63}$$

As a result, the dissipation rate density (15) becomes

$$J_e D = \left(\underset{\sim}{\boldsymbol{\Pi}}^{e} - \rho_i \frac{\partial \psi}{\partial \underset{\sim}{\boldsymbol{E}}^{e}}\right) : \dot{\underset{\sim}{\boldsymbol{E}}}^{e} + \left(J_e a - \rho_i \frac{\partial \psi}{\partial {}^{\chi}d}\right) \dot{{}^{\chi}d} + \left(J_e \underline{\boldsymbol{b}} \cdot \underset{\sim}{\boldsymbol{F}}^{-T} - \rho_i \frac{\partial \psi}{\partial \boldsymbol{\nabla}_X {}^{\chi}d}\right) \cdot \boldsymbol{\nabla}_X \dot{{}^{\chi}d} + \underset{\sim}{\boldsymbol{\Pi}}^{M} : \dot{\underset{\sim}{\boldsymbol{F}}}^{i} \underset{\sim}{\boldsymbol{F}}^{i-1} - \rho_i \frac{\partial \psi}{\partial \alpha} \dot{\alpha} \geqslant 0 \tag{64}$$

As in Section 2.2, the most simple version of the model consists in assuming that the additional degree of freedom and its gradient are not associated with dissipative mechanisms. As a result, we obtain the following state laws:

$$a = \rho \frac{\partial \psi}{\partial {}^{\chi}d}, \quad \underline{\boldsymbol{b}} = \rho \frac{\partial \psi}{\partial \boldsymbol{\nabla}_x {}^{\chi}d} \cdot \underset{\sim}{\boldsymbol{F}}^{T} \tag{65}$$

in addition to $(19)_1$. The residual dissipation then reads

$$J_e D = \underset{\sim}{\boldsymbol{\Pi}}^{M} : \dot{\underset{\sim}{\boldsymbol{F}}}^{i} \underset{\sim}{\boldsymbol{F}}^{i-1} - R\dot{\alpha} \geqslant 0 \tag{66}$$

where R is the generic name for the thermodynamic force associated with internal variables and still given by (20). Introducing a dissipation potential, $\Omega(\underset{\sim}{\boldsymbol{\Pi}}^M, R)$, the evolution equations for inelastic flow and internal variables can be formulated as follows:

$$\dot{\underset{\sim}{\boldsymbol{F}}}^i \underset{\sim}{\boldsymbol{F}}^{i-1} = \frac{\partial \Omega}{\partial \underset{\sim}{\boldsymbol{\Pi}}^M}, \quad \dot{\alpha} = -\frac{\partial \Omega}{\partial R} \tag{67}$$

Yield functions are now introduced for crystal plasticity, $f^s(\underset{\sim}{\boldsymbol{\Pi}}^M, r^s)$, on the one hand, and for damage, $f_c^s(\underset{\sim}{\boldsymbol{\Pi}}^M, Y^s)$, on the other hand, where r^s and Y^s are the corresponding yield limits for both families of criteria. The plastic component of the flow rule is written at the slip system level, while the damage components will be defined on crystallographic damage planes. Plastic deformation takes place through the slip processes associated to the N slip systems characterized by the slip direction $\underline{\boldsymbol{l}}^s$ and the slip plane normal $\underline{\boldsymbol{n}}^s$ defined for the system s. Cleavage damage is represented by the opening δ_c^s of crystallographic cleavage planes with the normal vector $\underline{\boldsymbol{n}}_c^s$. Additional damage systems are introduced for the in-plane accommodation along orthogonal directions $\underline{\boldsymbol{l}}_1^s$ and $\underline{\boldsymbol{l}}_2^s$, once crack opening has started. δ_c^s, δ_1^s and δ_2^s are strain like variables that account in a continuum way for micro-cracking inside the volume element under mode I, mode II and mode III loading conditions, respectively, and N_c stands for the number of damage planes which are fixed crystallographic planes depending on the crystal structure. The corresponding yield functions are

$$f^s(\underset{\sim}{\boldsymbol{\Pi}}^M, \tau_c^s) = |\underset{\sim}{\boldsymbol{\Pi}}^M : \underset{\sim}{\boldsymbol{P}}^s| - \tau_c^s, \quad \text{with } \underset{\sim}{\boldsymbol{P}}^s = \underline{\boldsymbol{l}}^s \otimes \underline{\boldsymbol{n}}^s, \quad 1 \leqslant s \leqslant N \tag{68}$$

$$f_c^s(\underset{\sim}{\boldsymbol{\Pi}}^M, \tau_c^s) = |\underset{\sim}{\boldsymbol{\Pi}}^M : \underset{\sim}{\boldsymbol{P}}_c^s| - Y, \quad \text{with } \underset{\sim}{\boldsymbol{P}}_c^s = \underline{\boldsymbol{n}}_c^s \otimes \underline{\boldsymbol{n}}_c^s, \quad 1 \leqslant s \leqslant N_c \tag{69}$$

$$f_{1,2}^s(\underset{\sim}{\boldsymbol{\Pi}}^M, \tau_c^s) = |\underset{\sim}{\boldsymbol{\Pi}}^M : \underset{\sim}{\boldsymbol{P}}_{1,2}^s| - Y, \quad \text{with } \underset{\sim}{\boldsymbol{P}}_{1,2}^s = \underline{\boldsymbol{l}}_{1,2}^s \otimes \underline{\boldsymbol{n}}_c^s, \quad 1 \leqslant s \leqslant N_c \tag{70}$$

The driving force for cleavage plane opening therefore is the normal stress to the cleavage plane, $\underline{\boldsymbol{n}}_c^s \cdot \underset{\sim}{\boldsymbol{\Pi}}^M \cdot \underline{\boldsymbol{n}}_c^s$. The same threshold, Y, is used for all 3 damage mechanisms. Specific conditions must be added to handle unilateral damage. Such conditions have been described in Aslan et al. (2011) and are not presented here because only simulations under monotonic loading are considered. In particular, the condition that crack opening, δ_c^s, cannot be negative, is enforced.

The dissipation potential is the sum of the individual contributions:

$$\Omega = \sum_{s=1}^{N} \Omega^s(f_s, \tau_c^s) + \sum_{s=1}^{N_c} \left(\Omega_c^s(f_c^s) + \Omega_1^s(f_1^s) + \Omega_2^s(f_2^s)\right) \tag{71}$$

The kinematics of plastic slip and damage follows:

$$\dot{\underset{\sim}{\boldsymbol{F}}}^i \cdot \underset{\sim}{\boldsymbol{F}}^{i-1} = \sum_{s=1,N} \dot{\gamma}^s \underset{\sim}{\boldsymbol{P}}^s + \sum_{s=1}^{N_c} \left(\dot{\delta}_c^s \underset{\sim}{\boldsymbol{P}}_c^s + \dot{\delta}_1^s \underset{\sim}{\boldsymbol{P}}_1^s + \dot{\delta}_2^s \underset{\sim}{\boldsymbol{P}}_2^s\right) \tag{72}$$

with

$$\dot{\gamma}^s = \frac{\partial \Omega^s}{\partial \underset{\sim}{\boldsymbol{\Pi}}^M} \operatorname{sign}\left(\underset{\sim}{\boldsymbol{\Pi}}^M : \underset{\sim}{\boldsymbol{P}}^s\right), \quad \dot{\delta}_c^s = \frac{\partial \Omega_c^s}{\partial \underset{\sim}{\boldsymbol{\Pi}}^M} \operatorname{sign}\left(\underset{\sim}{\boldsymbol{\Pi}}^M : \underset{\sim}{\boldsymbol{P}}_c^s\right), \quad \dot{\delta}_{1,2}^s = \frac{\partial \Omega_{1,2}^s}{\partial \underset{\sim}{\boldsymbol{\Pi}}^M} \operatorname{sign}\left(\underset{\sim}{\boldsymbol{\Pi}}^M : \underset{\sim}{\boldsymbol{P}}_{1,2}^s\right) \tag{73}$$

Note that the trace of $\dot{\underset{\sim}{\boldsymbol{F}}}^i \cdot \underset{\sim}{\boldsymbol{F}}^{i-1}$ does not vanish due to the kinematics of cleavage plane opening $\underset{\sim}{\boldsymbol{P}}_c^s$. Damage is therefore associated with volume changes in a way similar to classical ductile damage models (Besson, 2009).

At this stage, the meaning of the microdamage variable, ${}^{\chi}d$, has still not been defined. It will be related to an additional scale internal variable, d, that will be shown to measure the total amount of cumulative damage. A quadratic free energy potential is then chosen which allows for a proper coupling between plasticity and damage:

$$\rho_i \psi(\underset{\sim}{\boldsymbol{E}}^e, \varrho^s, d, {}^{\chi}d, \nabla_X {}^{\chi}d) = \frac{1}{2} \underset{\sim}{\boldsymbol{E}}^e : \underset{\approx}{\boldsymbol{C}} : \underset{\sim}{\boldsymbol{E}}^e + r_0 \sum_{s=1}^{N} \varrho^s + \frac{1}{2} q \sum_{r,s=1}^{N} h^{rs} \varrho^r \varrho^s + \sigma_0^c d \exp\left(-\Theta \sum_{s=1}^{N} \varrho^s\right) + \frac{1}{2} H d^2 + \frac{1}{2} {}^{\chi}H (d - {}^{\chi}d)^2 + \frac{1}{2} A \nabla_X {}^{\chi}d \cdot \nabla_X {}^{\chi}d$$

where r_0, q, H, ${}^{\chi}H$ and A are scalar material constants. Coupling between plasticity and damage is controlled by parameter Θ. The ϱ^s variables are standard isotropic work-hardening variables for crystal plasticity, that can be related to dislocation densities, q being the usual nonlinear hardening modulus, and h^{rs}, the interaction matrix (taken as the identity in the case of nickel-base superalloys considered in the next section). The initial critical resolved shear stress for the activation of plastic slip is r_0. The coupling parameter ${}^{\chi}H$ represents a penalty term that forces the microvariable ${}^{\chi}d$ to follow the cumulative damage variable, d, in the spirit of the micromorphic approach (Forest, 2009). The parameter A (unit MPa mm^2) contains the characteristic length of the medium. The state laws take the form:

$$\underset{\sim}{\boldsymbol{\Pi}}^e = \rho_i \frac{\partial \psi}{\partial \underset{\sim}{\boldsymbol{E}}^e} = \underset{\approx}{\boldsymbol{C}} : \underset{\sim}{\boldsymbol{E}}^e \tag{74}$$

$$\tau_c^s = \rho_i \frac{\partial \psi}{\partial \varrho^s} = r_0 + q \sum_{r=1}^{N} h^{sr} \varrho^s - \sigma_0^c \Theta d \exp\left(-\Theta \sum_{l=1}^{N} \varrho^l\right) \tag{75}$$

$$Y = \rho_i \frac{\partial \psi}{\partial d} = \sigma_0^c \exp\left(-\Theta \sum_{l=1}^{N} \varrho^l\right) + Hd + {}^{\chi}H(d - {}^{\chi}d) \tag{76}$$

$$a = \rho \frac{\partial \psi}{\partial {}^{\chi}d} = -{}^{\chi}H(d - {}^{\chi}d), \quad \underline{\boldsymbol{b}} = \rho \frac{\partial \psi}{\partial \nabla {}^{\chi}d} = A \nabla_X {}^{\chi}d \cdot \underset{\sim}{\boldsymbol{F}}^T \tag{77}$$

The thermodynamic force, Y, enters the threshold of the yield functions (69) and (70). Damage starts when the normal stress component to one cleavage plane $1 \leqslant s \leqslant N_c$ reaches the threshold:

$$Y_0 := \sigma_0^c e^{-\Theta \gamma_{cum}}, \quad \text{with } \gamma_{cum} := \sum_{l=1}^{N} \varrho^l \tag{78}$$

where γ_{cum} represents cumulative plastic slip, as it will become clear from the evolution rule for ϱ^s in Eq. (79). In the absence of plasticity, the fracture stress σ_0^c is very high and corresponds to the cleavage stress. It is well-known that in BCC and HCP crystals the cleavage stress is reduced by the accumulation of plasticity (Parisot et al., 2004). This is the origin of the coupling between plasticity and damage. Once damage has started, a negative modulus H induces localization of damage into a crack-like zone in a region of the component. Plastic strain also localizes due to the softening induced by damage in the hardening rule (75).

The evolution laws of the internal variables ϱ^s and d, that are associated with dissipation, are

$$\dot{\varrho}^s = -\frac{\partial \Omega}{\partial \tau_c^s} = \frac{\partial \Omega}{\partial f^s} \frac{\partial f^s}{\partial \tau_c^s} = |\dot{\gamma}^s| \tag{79}$$

$$\dot{d} = -\frac{\partial \Omega}{\partial Y} = \sum_{i=1}^{N_c} \frac{\partial \Omega_c^s}{\partial f_c^s} \frac{\partial f_c^s}{\partial Y} = \sum_{s=1}^{N_c} \left(|\dot{\delta}_c^s| + |\dot{\delta}_1^s| + |\dot{\delta}_2^s|\right) \tag{80}$$

Due to the chosen quadratic potential, the variable ϱ^s turns out to be nothing but the cumulative slip on slip system s. According to the normality rule, the damage variable d is found to be equal to the cumulative damage strain on the cleavage systems. It is a measure of the total amount of damage corresponding to micro-crack opening and shearing. The residual dissipation finally is

$$J_e D = \sum_{s=1}^{N} \tau_c^s \dot{\varrho}^s + Y\dot{d} \geqslant 0 \tag{81}$$

3.3. Finite element simulation of crack propagation in single crystals

A small strain version of the previous model has been implemented in a finite element code following the method proposed in Aslan and Forest (2009). Quadratic elements with reduced integration have been retained, displacement and micro-damage degrees of freedom being attributed to each node. 2D finite element simulations under plane strain conditions are presented in this section. The capacity of the model to provide mesh-independent results has been demonstrated in Aslan and Forest (2009).

In the present work, a 2D single crystal CT-like specimen under monotonic tension is analyzed with an horizontal cleavage plane. The corresponding finite element mesh is given in Fig. 4. Analyses are performed for two different crack widths, obtained by furnishing different material values of parameter A, which controls the size of the crack width for the same boundary conditions. As it is demonstrated in Fig. 5 larger crack widths can be obtained resulting in shorter crack lengths for the same macro opening.

The main advantage of the proposed model is to consider simultaneously several possible fracture planes so that complicated crack paths can be predicted, including crack bifurcation or branching. Fig. 6 presents the analysis result for the same geometry as Fig. 4 under monotonic tension but with two orthogonal planes oriented at 45° replacing the previous horizontal single cleavage plane. The two orthogonal fracture lines stand for the traces of {1 1 1} planes on the (0 0 1) plane of computation. Such {1 1 1} fracture planes are relevant in the case of BCC and FCC single crystals. The computation also accounts for the slip systems for crystal plasticity in FCC crystals. The vertical direction is a [0 1 0] crystal direction while the horizontal direction is [1 0 0]. The figure shows that the crack starts with branching and one of the branches dominates for further opening, thus validating that the model is able to predict crack branching and bifurcation, as observed for instance in single crystal nickel-base superalloys (Flouriot et al., 2003). The simulation of a straight crack path is possible when both damage systems cooperate. Finite elements are considered as broken when the driving force for damage, Y is below an ultimate stress value of 0.01 MPa. The typical stress distribution at a crack tip was found at the tip of the dominating crack at the different stages.

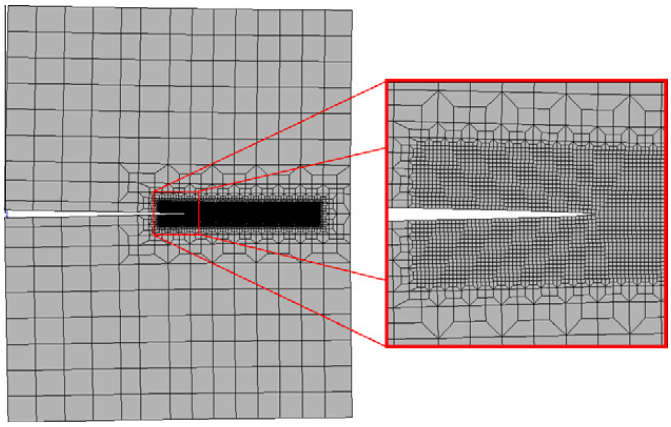

Fig. 4. Finite element mesh of a CT-like specimen. Mesh refinement is required in the crack propagation zone.

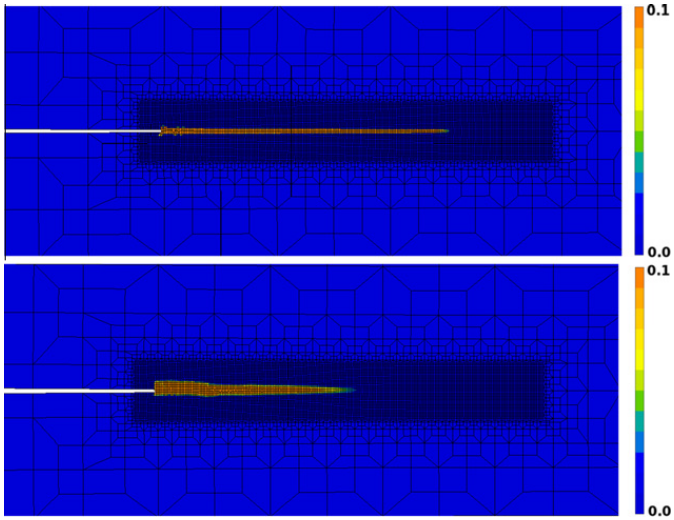

Fig. 5. Crack growth in a 2D single crystal CT-like specimen with a single cleavage plane aligned through the horizontal axis under vertical tension. Field variable d. (Top) $A = 100$ MPa mm^2, $H = -20{,}000$ MPa, ${}^{\chi}H = 30{,}000$ MPa, (bottom) $A = 150$ MPa mm^2, $H = -10{,}000$ MPa, ${}^{\chi}H = 30{,}000$ MPa.

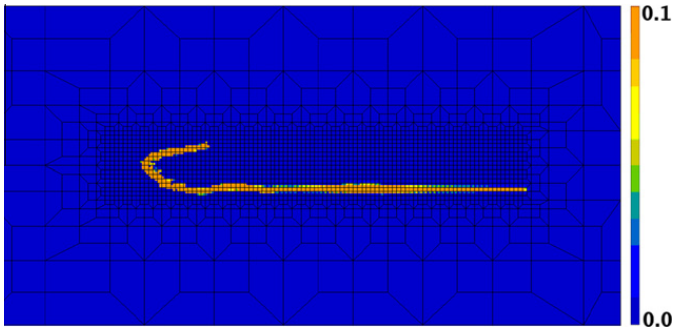

Fig. 6. Crack growth in a 2D single crystal CT-like specimen under tension with two orthogonal cleavage planes oriented at 45°. Field variable d. $A = 100$ MPa mm^2, $H = -20{,}000$ MPa, ${}^{\chi}H = 30{,}000$ MPa.

Crack initiation and growth take place only when sufficient plastic strain has taken place in the crack tip zone. Material parameters of the model can be calibrated in order to favor straight crack growth or branching, which is necessary for describing the real behavior of cracks in nickel-base superalloys at different temperatures (Wen & Yue, 2007).

4. Conclusion

The micromorphic approach amounts to selecting a constitutive variable, ϕ, in a mechanical continuum model and to introduce an associated microvariable, ${}^{\chi}\phi$, and its gradient, $\nabla_X {}^{\chi}\phi$, in the extended continuum theory (Forest, 2009). In Erin-

gen (1999), it is applied to the deformation itself, $\phi \equiv \boldsymbol{F}$, thus introducing the microdeformation, ${}^{\chi}\phi \equiv \boldsymbol{\chi}$. The departure of the microstructure from the macromotion is represented symbolically by the difference, ${}^{\chi}\phi - \phi$, and corresponds to an energetic cost in the free energy function. In the case of crystal plasticity, we have proposed in this work to consider the plastic microdeformation, ${}^{\chi}\phi \equiv \hat{\boldsymbol{\chi}}^{p}$, associated with the plastic deformation $\boldsymbol{F}^{p}$. The relative plastic deformation, $\boldsymbol{e}^{p} = \boldsymbol{F}^{p-1} \cdot \hat{\boldsymbol{\chi}}^{p}$, measures the difference between the micro and macro-plastic deformation. As long as this difference remains small, the curl of the plastic microdeformation is close to the dislocation density tensor, representing plastic incompatibility in the crystal. The *microcurl* models represents the restriction of the micromorphic model to the rotational part of the microdeformation, instead of the full gradient. The simple example of a two-phase laminate microstructure undergoing single slip provides explicit scaling laws for the yield strength of the material as a function of microstructure characteristic size. Material parameters can be identified so as to recover scaling exponents from 0 to -2, including the scaling laws, $l^{-1/2}$ and l^{-1}, respectively known as Hall–Petch and Orowan relationships. In contrast, the strain gradient plasticity model obtained as a limit case of the *microcurl* theory when the internal constraint $\boldsymbol{e}^{p} \equiv 0$ is enforced, delivers a unique scaling law with a power -2, without direct physical meaning, to the knowledge of the authors.

The micromorphic approach has then been applied to a damage variable, $\phi \equiv d$, representing the cumulative opening and shearing modes of microcracks in a single crystal material volume element. The corresponding microvariable, ${}^{\chi}d$, and its gradient, are used as a regularization method for mesh-insensitive simulation of crack propagation in ductile single crystals. The main interest of the model is that the crack path is not predefined and rather is an outcome of the simulation. Crack opening is allowed with respect to {1 1 1} planes in FCC crystals. In the two-dimensional situation, two crack planes are possible and allow crack branching and crack bifurcation, but also a straight crack path when both mechanisms cooperate.

The results obtained in this work illustrate the potential of micromorphic models to handle in a generic way size effects in crystals. However, the effects shown remain qualitative and there is still a long way to obtain quantitative agreement with experimental data. For instance, the linear kinematic component generated by the *microcurl* model is unrealistic and more general constitutive equations between higher order stresses and the microdeformation gradient will be necessary to represent non-linear kinematic hardening. In the context of multiple slip, size-dependent isotropic hardening is also expected and not accounted for in the present version of the model.

Promising results were presented for the simulation of crack propagation in single crystals under monotonic loading. Crack propagation under cyclic loading also is of the utmost important, especially for single crystal nickel-base superalloys used in turbine blades, and extensions of the presented constitutive framework allow for the simulation of cyclic crack propagation, including some crack closure effects by introducing unilateral damage in the modeling (Aslan et al., 2011). Material parameters of the damage model can be identified from experimental crack growth rate, whereas the characteristic length of the model mainly controls branching vs. straight propagation.

References

Acharya, A. (2004). Constitutive analysis of finite deformation field dislocation mechanics. *Journal of the Mechanics and Physics of Solids, 52*, 301–316.

Aifantis, E. C. (1984). On the microstructural origin of certain inelastic models. *Journal of Engineering Materials and Technology, 106*, 326–330.

Aslan, O., Quilici, S., & Forest, S. (2011). Numerical modeling of fatigue crack growth in single crystals based on microdamage theory. *International Journal of Damage Mechanics*.

Aslan, O., & Forest, S. (2009). Crack growth modelling in single crystals based on higher order continua. *Computational Materials Science, 45*, 756–761.

Besson, J. (2009). Damage of ductile materials deforming under multiple plastic or viscoplastic mechanisms. *International Journal of Plasticity, 25*, 2204–2221.

Chen, Y., & Lee, J. D. (2003). Connecting molecular dynamics to micromorphic theory. (I) Instantaneous and averaged mechanical variables. *Physica A, 322*, 359–376.

Claus, W. D., & Eringen, A. C. (1969). Three dislocation concepts and micromorphic mechanics. In *Developments in mechanics, Proceedings of the 12th midwestern mechanics conference* (Vol. 6, pp. 349–358).

Claus, W. D., & Eringen, A. C. (1971). Dislocation dispersion of elastic waves. *International Journal of Engineering Science, 9*, 605–610.

Clayton, J. D., Bamman, D. J., & McDowell, D. L. (2005). A geometric framework for the kinematics of crystals with defects. *Philosophical Magazine, 85*, 3983–4010.

Cordero, N. M., Gaubert, A., Forest, S., Busso, E., Gallerneau, F., & Kruch, S. (2010). Size effects in generalised continuum crystal plasticity for two-phase laminates. *Journal of the Mechanics and Physics of Solids, 58*, 1963–1994.

Eringen, A. C. (1999). *Microcontinuum field theories*. New York: Springer.

Eringen, A. C., & Claus, W. D. (1970). A micromorphic approach to dislocation theory and its relation to several existing theories. In J. Simmons, R. de Wit, & R. Bullough (Eds.). *Fundamental aspects of dislocation theory* (vol. 317 II, pp. 1023–1062). Nat. Bur. Stand. (US) Spec. Publ.

Flouriot, S., Forest, S., Cailletaud, G., Köster, A., Rémy, L., Burgardt, B., et al (2003). Strain localization at the crack tip in single crystal CT specimens under monotonous loading: 3D finite element analyses and application to nickel-base superalloys. *International Journal of Fracture, 124*, 43–77.

Forest, S. (2008). Some links between Cosserat, strain gradient crystal plasticity and the statistical theory of dislocations. *Philosophical Magazine, 88*, 3549–3563.

Forest, S. (2009). The micromorphic approach for gradient elasticity, viscoplasticity and damage. *ASCE Journal of Engineering Mechanics, 135*, 117–131.

Forest, S., Barbe, F., & Cailletaud, G. (2000). Cosserat modelling of size effects in the mechanical behaviour of polycrystals and multiphase materials. *International Journal of Solids and Structures, 37*, 7105–7126.

Forest, S., & Sievert, R. (2003). Elastoviscoplastic constitutive frameworks for generalized continua. *Acta Mechanica, 160*, 71–111.

Forest, S., & Sievert, R. (2006). Nonlinear microstrain theories. *International Journal of Solids and Structures, 43*, 7224–7245.

Germain, P. (1973). The method of virtual power in continuum mechanics. Part 2: Microstructure. *SIAM Journal of Applied Mathematics, 25*, 556–575.

Grammenoudis, P., Tsakmakis, C., & Hofer, D. (2009). Micromorphic continuum Part II: Finite deformation plasticity coupled with damage. *International Journal of Non-Linear Mechanics, 44*, 957–974.

Günther, W. (1958). Zur statik und kinematik des cosseratschen kontinuums. *Abhandlungen der Braunschweigischen Wissenschaftlichen Gesellschaft, 10*, 195–213.

Gurtin, M. E. (2002). A gradient theory of single-crystal viscoplasticity that accounts for geometrically necessary dislocations. *Journal of the Mechanics and Physics of Solids, 50*, 5–32.

Gurtin, M. E., & Anand, L. (2009). Thermodynamics applied to gradient theories involving the accumulated plastic strain: The theories of Aifantis and Fleck & Hutchinson and their generalization. *Journal of the Mechanics and Physics of Solids, 57*, 405–421.
Hirschberger, C. B., & Steinmann, P. (2009). Classification of concepts in thermodynamically consistent generalized plasticity. *ASCE Journal of Engineering Mechanics, 135*, 156–170.
Kröner, E. (1963). On the physical reality of torque stresses in continuum mechanics. *International Journal of Engineering Science, 1*, 261–278.
Kröner, E. (1969). Initial studies of a plasticity theory based upon statistical mechanics. In M. Kanninen, W. Adler, A. Rosenfield, & R. Jaffee (Eds.), *Inelastic behaviour of solids* (pp. 137–147). McGraw-Hill.
Lazar, M., & Maugin, G. A. (2004). Dislocations in gradient micropolar – I: Screw dislocation. *Journal of the Mechanics and Physics of Solids, 52*, 2263–2284.
Lazar, M., Maugin, G. A., & Aifantis, E. (2006). Dislocations in second strain gradient elasticity. *International Journal of Solids and Structures, 43*, 1787–1817.
Lee, J. D., & Chen, Y. (2003). Constitutive relations of micromorphic thermoplasticity. *International Journal of Engineering Science, 41*, 387–399.
Mandel, J. (1973). Equations constitutives et directeurs dans les milieux plastiques et viscoplastiques. *International Journal of Solids Structures, 9*, 725–740.
Musienko, A., & Cailletaud, G. (2009). Simulation of inter- and transgranular crack propagation in polycrystalline aggregates due to stress corrosion cracking. *Acta Materialia, 57*, 3840–3855.
Parisot, R., Forest, S., Pineau, A., Nguyen, F., Démonet, X., & Mataigne, J.-M. (2004). Deformation and damage mechanisms of zinc coatings on galvanized steel sheets, Part II: Damage modes. *Metallurgical and Materials Transactions, 35A*, 813–823.
Peerlings, R. H. J., Massart, T. J., & Geers, M. G. D. (2004). A thermodynamically motivated implicit gradient damage framework and its application to brick masonry cracking. *Computer Methods in Applied Mechanics and Engineering, 193*, 3403–3417.
Regueiro, R. A. (2010). On finite strain micromorphic elastoplasticity. *International Journal of Solids and Structures, 47*, 786–800.
Sansour, C., Skatulla, S., & Zbib, H. (2010). A formulation for the micromorphic continuum at finite inelastic strains. *International Journal of Solids Structures, 47*, 1546–1554.
Steinmann, P. (1996). Views on multiplicative elastoplasticity and the continuum theory of dislocations. *International Journal of Engineering Science, 34*, 1717–1735.
Teodosiu, C., & Sidoroff, F. (1976). A theory of finite elastoviscoplasticity of single crystals. *International Journal of Engineering Science, 14*, 165–176.
Wen, Z. X., & Yue, Z. F. (2007). Fracture behaviour of the compact tension specimens of nickel-based single crystal superalloys at high temperature. *Materials Science and Engineering A, 456*, 189–201.